Continuum Mech. Thermodyn. (2023) 35:1735–1744
https://doi.org/10.1007/s00161-023-01199-8

ORIGINAL ARTICLE

Mahmoud Kadkhodaei · Marek Pawlikowski · Rafał Drobnicki · Janusz Domański

Modeling of hyperelasticity in polyamide 12 produced by selective laser sintering

Received: 27 December 2022 / Accepted: 27 January 2023 / Published online: 24 February 2023

Abstract Polyamide 12 (PA12) is a core material in many 3D-printing techniques, including selective laser sintering (SLS), and its mechanical characterization helps to better understand behaviors of additively manufactured parts made from this polymer. In this paper, the elastic response of SLS-produced PA12 is shown to be nonlinear. Standard test samples with different orientations with regard to the scanning direction are 3D-printed with the use of PA2200 powder, and their elastic response is investigated under uniaxial tension at different strain rates. Mooney–Rivlin hyperelastic models are proposed to address the observed nonlinear elasticity of the samples. Cyclic response of the specimens is shown to be stabilized after a few transient cycles so the material parameters are determined for trained samples after shakedown in their response. The obtained parameters are found to depend on the loading speed; thus, a rate-dependent hyperelastic constitutive model is presented for PA12 produced by selective laser sintering. This model is validated by comparing its numerical prediction with empirical responses under simple tension tests.

Keywords Selective laser sintering · SLS · Polyamide 12 · PA12 · Hyperelastic model

1 Introduction

Polyamide 12 (PA12 or Nylon-12) has been vastly utilized in several 3D-printing methods such as Selective Laser Sintering (SLS) due to its large processing window between the crystallization and the melting temperatures [1,2]. SLS-produced polyamide parts have been employed in various areas including offshore applications [3], automotive industry [4], and bioengineering [5–7]. Pantographic lattice structures, which contain intersecting arrays of parallel fibers, are also usually fabricated by selective laser sintering of PA12. The arrays are interconnected by pivots, and this configuration makes pantographs undergo very large deformations, leading to their high toughness. This also gives rise to an outstanding strength-to-weight ratio. Pantographic structures can be considered mathematically-driven metamaterials [8–10] whose responses can be tuned by adjustments in their geometry and properties of their construction. Successful applications of such products need thorough investigations on their fabrication, characterization, and modeling; thus, numerous works have been so far done on different aspects of these topics from different points of view [11–16].

The first work on basic phenomena regarding powder properties and fabrication parameters in selective laser sintering of polymers was conducted by Gibson and Shi [17]. They studied the influence of part bed

Communicated by Andreas Öchsner.

M. Kadkhodaei
Department of Mechanical Engineering, Isfahan University of Technology, Isfahan 84156-83111, Iran

M. Pawlikowski (✉)· R. Drobnicki · J. Domański
Institute of Mechanics and Printing, Warsaw University of Technology, ul. Narbutta 85, 02-524 Warszawa, Poland
E-mail: marek.pawlikowski@pw.edu.pl

temperature, laser power, scan size and spacing, slice thickness, building orientation, and post-processing including coating and surface finishing on the relative density, tensile strength, and surface hardness of the products. Since then, each of such details has been more deeply discussed in other investigations. An SLS-produced part is generally a mixture of fully melted and partially melted polymer; thus, the so-called Degree of Particle Melt (DMP) has considerable effects on mechanical properties since it affects crystallinity percentage [18,19]. Accordingly, relative density, bulk and surface strength, and dimensional accuracy of the products depend on laser energy density and scanning speed [20,21], which determine DMP. There are also reports on the influence of thickness on the mechanical properties of selective laser-sintered PA12 because spatial distribution and morphological characteristics of probable pores inside the product are shown to vary with thickness [22,23].

The point-wise manufacturing in SLS may give rise to poor densification and, hence, the formation of pores in the products [24]. Since the morphology, dimensions, and distribution of such pores are different for different build directions, the mechanical properties of SLS-produced parts may show dependencies on the printing orientation [25]. Another reason for such a possible anisotropy is the layered manufacturing owing to which differences in bond strength within each layer and between two adjacent ones occur, and these differences are not the same for all build directions [26]. An additional hypothesis is that direction-dependency is due to different thermal histories for different built orientations [27]. The outcome of these effects altogether is the potential of anisotropy in the mechanical properties of selective laser-sintered products; however, different extents of anisotropy have been reported in different studies [28]. While considerable anisotropies are found in some studies [29], negligible direction dependencies are seen in some others [30]. In particular, the elastic response of SLS parts for all print directions has been shown to be nearly identical for a specified loading speed [26,31]. Moreover, if recycled powders are not used, the anisotropy is proved to be significantly suppressed [32,33].

In 3D-printing of a specified material, whether the product is designed to be dense, porous, or a cellular lattice structure, several investigations on different manufacturing techniques and various types of polymers as well as metals have shown that the obtained behaviors vary by varying the process parameters [34,35]. Consequently, for theoretical studies on the mechanical responses of additively manufactured products, the constitute equations and mechanical properties of the base material should be directly determined by examining bulk specimens that are 3D-printed with the same production parameters [36,37]. Modeling and numerical simulation of SLS-produced PA12 parts have been mainly conducted for pantographic structures under monotonic loadings [38], and various issues have been investigated by usually assuming linear elastic response for the material [8,39]. However, characterizations of Polyamide 12 have shown several kinds of material nonlinearity such as elastoplasticity [25], viscoelasticity [40], viscoplacticity [41], and viscoelastoplasticity [26]. Yang et al. [42] showed that even the elastic part of the response is not linear so nonlinear elasticity is required to be employed when studying the elastic response of SLS-produced PA12 parts such as pantographs. They cut samples from a pantographic structure and conducted uniaxial tensile tests. Founded on the calculated strain energy from the experimental stress–strain response, they determined the required material parameters of different hyperelastic models and examined their numerical predications compared with empirical results for shear test of the pantographic structure.

The main aim of the present work is to improve available findings on nonlinear elasticity of SLS-produced Polyamide 12. Standard samples for simple tension test are manufactured by selective laser sintering of PA2200 powder. Different build orientations are chosen, and the elastic response of the specimens is investigated under uniaxial tension at different strain rates. Negligible direction-dependency but clear nonlinearity is seen in the obtained results; thus, different Mooney–Rivlin hyperelastic models are examined to determine which one more appropriately reproduces the empirical results. Cyclic response of the specimens shows shakedown after a limited number of transient cycles; thus, determination of the material parameters is conducted for the stabilized cycle. The material parameters are shown to be dependent on the loading speed. Consequently, rate-dependent hyperelastic models for SLS-produced PA12 are presented.

2 Materials and methods

Polyamide PA2200 powder with the average grain size of 56 μm provided by EOS GmbH-Electro Optical Systems was utilized in selective laser sintering machine FORMIGA P 100 equipped with 30 W CO_2 laser of 10.6 μm wavelength. Dog-bone samples, with the dimensions shown in Fig. 1, were manufactured for simple tension tests according to ISO-527 standard. To examine the effects of build direction on the tensile stress–strain response, as shown in Fig. 2, four different orientations for 3D-printing of the samples were chosen.

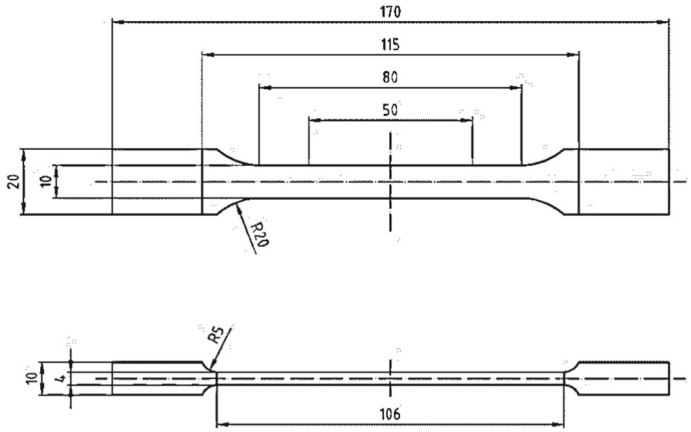

Fig. 1 Dimensions (in millimeters) of the standard test samples

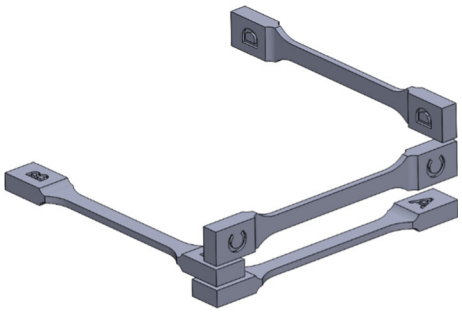

Fig. 2 Different orientations of the manufactured standard samples

The letters A, B, C, and D stand for the directions compared to the scanning direction. The longitudinal axis of samples A is along the scanning direction of the 3D printer.

To obtain every response for each direction, the corresponding experiment for each loading rate and specimen type was repeated three times to be assured of the repeatability of the empirical findings. Tension tests were carried out according to ISO-527 standard on an MTS Biosystem machine of the maximum load up to 25 kN. Extension of the gauge length during the experiments was recorded by means of an extensometer according to Fig. 3 in which the arranged test setup is shown. To study the effects of strain rate, three different loading speeds of 0.05, 0.5, and 5 mm/s were selected. Figure 4 shows a typical elastic response for direction C where the criterion of 0.2% strain offset is considered since the force-elongation curve clearly deviates from linearity compared to the dotted trend line. To address the observed nonlinearly, the theory of hyperelasticity is developed to model the elastic behavior of the SLS-produced Polyamide 12 specimens.

According to a formerly presented approach [43], the method of potential functions was applied to derive hyperelastic constitutive equations. This approach consists of formulation or selection of a scalar function relating a stress tensor with a strain tensor or their rate measurements (the function has got a physical sense of potential elasticity energy cumulated in a deformed medium). In our study, we assume that the material is homogeneous, isotropic and hyperelastic. We decided the Mooney–Rivlin (MR) potential function to be the best to model the mechanical behavior of the material:

$$\Psi = \sum_{p,q=0}^{n} c_{pq} \left(I_1 - 3\right)^p \left(I_2 - 3\right)^q, \tag{1}$$

where: I_1, I_2—first and second invariant of the right Cauchy tensor, respectively, c_{pq}—material constants with $c_{00} = 0$. We considered two forms of relationship (1), i.e., two-parameter (Eq. 2) and five-parameter (Eq. 3) MR models:

$$\Psi_1 = c_{10}\left(I_1 - 3\right) + c_{01}\left(I_2 - 3\right), \tag{2}$$

$$\Psi_2 = c_{10}\left(I_1 - 3\right) + c_{01}\left(I_2 - 3\right) + c_{20}\left(I_1 - 3\right)^2 + c_{11}\left(I_1 - 3\right)\left(I_2 - 3\right) + c_{02}\left(I_2 - 3\right)^2. \tag{3}$$

Fig. 3 Test setup to obtain tensile stress–strain responses of the specimens

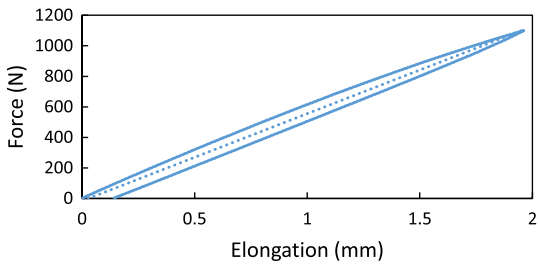

Fig. 4 Elastic loading–unloading curve for sample C at the loading speed of 0.05 mm/s

The constitutive equation was formulated with the use of the following equation:

$$S_{ij} = 2\frac{\partial \Psi}{\partial C_{ij}}, \tag{4}$$

where S_{ij}—second Piola-Kirchhoff stress tensor, C_{ij}—right Cauchy tensor. In the considered case of loading (uniaxial tensile tests), a non-zero stress component will be along the tensile force direction, namely S_{11}. Thus, the constitutive equation will show the change of stress S_{11} as the function of deformation defined by means of stretch ratio λ. The following forms of S_{11} were derived for the two potential functions Ψ_1 (5) and Ψ_2 (6):

$$S_{11} = \frac{2}{\lambda^4}\left(\lambda^3 - 1\right)\left(c_{01} + c_{10}\lambda\right), \tag{5}$$

$$S_{11} = \frac{2}{\lambda^5}\left(\lambda^3 - 1\right)\left(2c_{02} + 3c_{11}\lambda + c_{01}\lambda^2 - 6c_{02}\lambda^2 + 4c_{02}\lambda^3 + c_{10}\lambda^3 - 3c_{11}\lambda^2 - 3c_{11}\lambda^3 + 3c_{11}\lambda^4 + 4c_{20}\lambda^2 - 6c_{20}\lambda^3 + 2c_{20}\lambda^5\right). \tag{6}$$

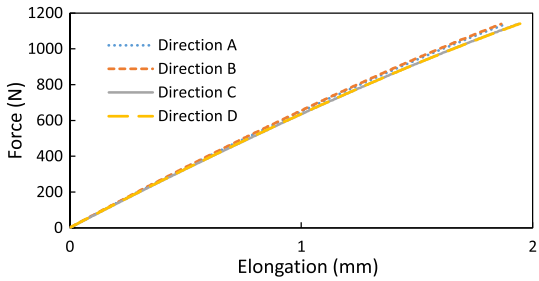

Fig. 5 Elastic tensile force-elongation responses of samples A to D at the loading speed of 0.05 mm/s

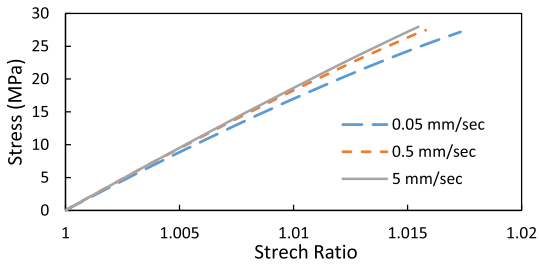

Fig. 6 Stress–stretch ratio responses for simple tension tests at three loadings speeds

All the constants in the above equations were determined based on experimental data by matching the theoretical curves described by (5) and (6) to the experimental measurements. The least square method was used, and the Marquardt algorithm was adopted to accomplish this task [44].

3 Results and discussion

The obtained elastic force-elongation responses for tension tests of samples A to D under the loading speed of 0.05 mm/s are illustrated in Fig. 5. As is seen, the curves are very close to each other, i.e., no considerable direction-dependency exists for the behaviors of the manufactured specimens. This independency was found for the other examined loading speeds as well. The observed isotropy is attributed to the well-calibrated SLS machine that is able to produce uniform samples with very low variations between different build orientations [5]. Moreover, considering similar studies on possible anisotropies in selectively laser sintered Polyamide 12 parts [26,31], the elastic responses of the examined specimens are expected to be nearly identical for all print directions. Results for the least studied loading speed of 0.05 mm/s are shown in Fig. 5, but the reported isotropy was observed for higher strain rates as well. However, for each built orientation, the obtained results depend on strain rate. Shown in Fig. 6 are the stress–stretch ratio curves for three loadings speeds of 0.05, 0.5, and 5 mm/s. Visually, a slight increase of Young's modulus is obtained by increasing the loading speed [26]. As a result, the material parameters of any constitutive model depend on strain rate, and this will be shown later in this work. Beforehand, it is worth noticing that the observed residual elongation in Fig. 4 at the end of a complete loading-unloading cycle leads to differences in the response of the subsequent cycles. As is seen in Fig. 7, for the studied SLS-produced Polyamide 12 samples, the transient responses converge to a stabilized response after 10 cycles; thus, shakedown phenomenon exists. In other words, the so-called *training* through an adequate number of cyclic loading should be conducted prior to any material characterization, modeling, identification, and practical application of selective laser sintered PA12 parts. The reported material parameters in this paper are determined for the stabilized response.

The material parameters of different MR models for the three examined loading speeds of 0.05, 0.5, and 5 mm/s are brought in Table 1. As expected from Fig. 6, for each parameter, the utilized Marquardt algorithm yields different values for different loading speeds. In other words, the present approach provides a strain rate-dependent constitutive model using which the observed nonlinear elasticity in SLS-produced Polyamide 12 can be studied.

To evaluate the validity of this approach, equivalent linear elastic response of the material is compared with available data in the literature. Based on the 2-parameter Mooney–Rivlin model, the modulus of rigidity

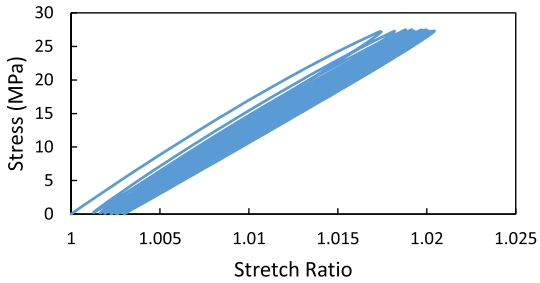

Fig. 7 Cyclic response at the loading speed of 0.05 mm/s until the stabilized cycle

Table 1 Material parameters of different versions of MR model for stabilized response of SLS-produced PA at different loading speeds

	0.05 mm/s		0.5 mm/s		5 mm/s	
Parameter (MPa)	2-Parameter model	5-Parameter model	2-Parameter model	5-Parameter model	2-Parameter model	5-Parameter model
c10	−4.32E+03	−6.28E+04	−1.48E+03	3.41E+03	5.39E+02	3.88E+04
c01	4.66E+03	6.33E+04	1.80E+03	−3.10E+03	−2.45E+02	−3.86E+04
c20		2.29E+09		−3.34E+08		−1.49E+09
c11		−4.66E+09		6.78E+08		3.04E+09
c02		2.38E+09		−3.44E+08		−1.55E+09

Table 2 The values of Young's modulus (GPa) at different loading conditions

	0.05 mm/s	0.5 mm/s	5 mm/s
First cycle	1.68	1.77	1.77
Tenth cycle	1.87	1.75	1.59

is 2 ($c_{10} + c_{01}$). For instance, at the loading speed of 0.05 mm/s, this leads to Young's modulus of around 1.87 GPa for the stabilized response. This number is in a good agreement with the reported elastic modulus of Polyamide 12 produced by selective laser sintering [45] and indicates that the proposed hyperelastic model in the present work predicts the elastic response of SLS-produced PA12 with a reasonable accuracy. To show the effects of strain rate as well as cycling on the mechanical properties, Young's moduli of the first and the tenth (stabilized) cycle for the three studied loading speeds are summarized in Table 2. For the first cycle, where the as-built specimens are loaded, Young's modulus is expected to slightly increase with an increase in the loading speed [26]. However, during cyclic loading, various phenomena happen that may lead to an unpredictable trend in variations of Young's modulus [46]: on the one hand, if significant damage is accumulated inside the structure, Young's modulus decreases in the course of cyclic loading. On the other hand, closure/compactness of microcracks and voids within the structure may occur during cycling. This makes the specimen stiffer against deformation and leads to an increase in Young's modulus. Therefore, the resultant of these two events is not easily predictable. Among several affecting parameters, loading frequency plays a pivotal role on the influence of each of these two reverse phenomena [46]. Consequently, once the stabilized response is achieved in the present study, it is seen in Table 2 that Young's modulus increases at the loading speed of 0.05 mm/s, almost remains the same at the loading speed of 0.5 mm/s, and decreases at the loading speed of 5 mm/s compared to the first cycle.

Comparison of the experimentally obtained stress-stretch ratio curves with the theoretically predicted responses for different loading speeds in Fig. 8 also verifies the presented approach in constitutive modeling of the material. As is seen, both examined versions of the MR model reproduce the empirical results with almost the same precision. Consequently, the 2-parameter model with less computational requirements suffices for practical purposes. The mathematical model of the PA12 material we are developing here can be utilized in modeling of pantographic structures printed by SLS technique. This form of the structures' modeling might be an alternative to other approaches, like homogenization method [47,48] or Cosserat approach with granular motif [49].

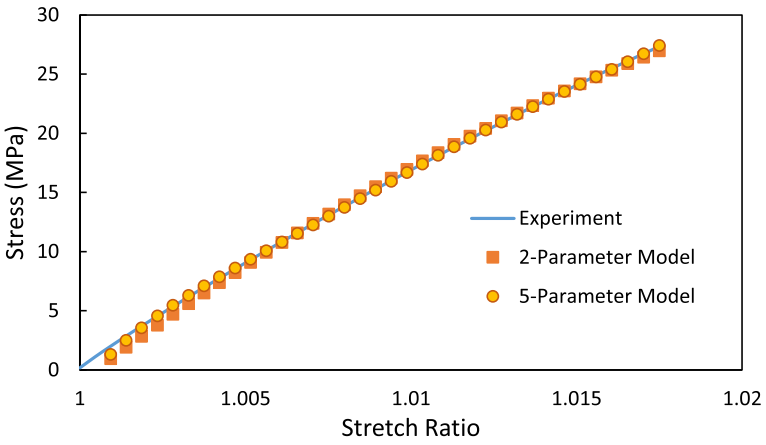

(a)

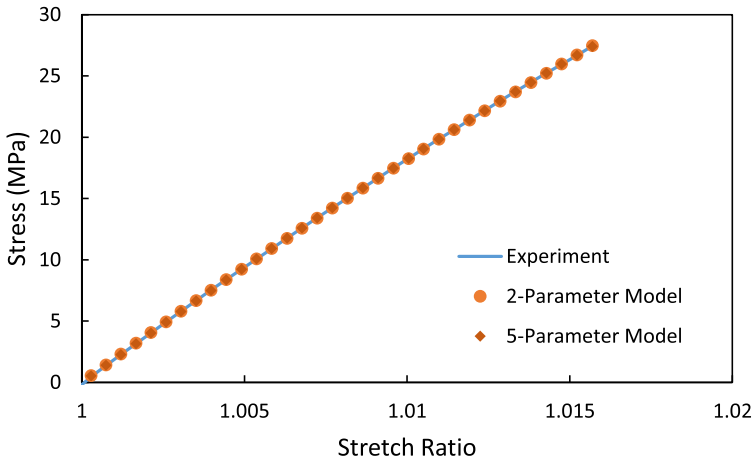

(b)

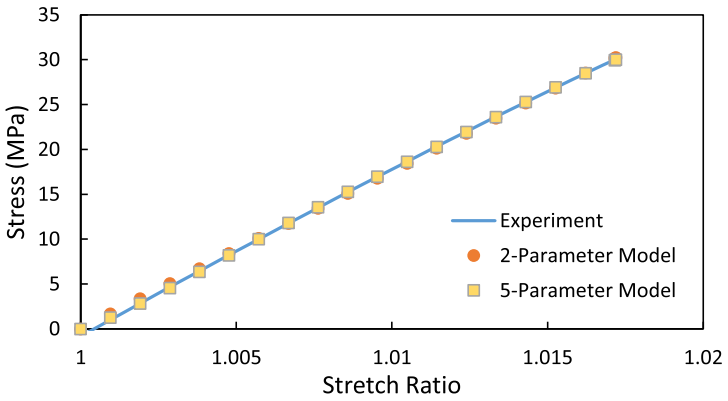

(c)

Fig. 8 Comparison of experimental results and numerical predictions of the Mooney–Rivlin model for the loading speed of **a** 0.05 mm/s, **b** 0.5 mm/s, and **c** 5 mm/s

4 Conclusions

The focus of this paper is hyperelastic modeling of SLS-produced Polyamide 12 to address nonlinear elasticity observed in simple tension test of standard samples. Two- and five-parameter Mooney–Rivlin models are examined, and both are found to be able to reproduce the empirically obtained results. Consequently, two-parameter Mooney–Rivlin hyperelastic model is sufficient in practice. Shakedown in cyclic loading is observed so that the material's response varies cycle by cycle but converges to a stabilized response after a limited number of transient cycles. Accordingly, training should be conducted on 3D-printed Polyamide 12 prior to any characterization, determination of material parameters, and practical application of such products. During training, the present findings show that Young's modulus may increase, remains almost unvaried, or decrease depending on the loading speed. Each model parameter is found to vary by varying the loading speed; thus, the proposed approach in this work provides a rate-dependent modeling scheme for nonlinear elasticity in SLS-produced PA 12 parts. The presented findings promote available knowledge on the mechanical behaviors of 3D-printed Polyamide 12 products such as pantographic structures. Extensions of this work are already planned to investigate inelastic responses as well.

Acknowledgements We wish to thank cordially our mentor and tutor, Prof. Tomasz Lekszycki, who passed away unexpectedly during preparation of this paper. He was always full of new and extraordinary ideas which he shared with us willingly. We will miss his clear mind and non-standard way of thinking. The first author is highly thankful to Polish Agency for Academic Exchange (NAWA) for their provided financial support under the Ulam NAWA program, Project No. BPN_ULM_2021_1_00284_U_00001.

References

1. Vasquez, M., Haworth, B., Hopkinson, N.: Optimum sintering region for laser sintered nylon-12. Proce. Inst. Mech. Eng. Part B J. Eng. Manuf. **225**(12), 2240–2248 (2011). https://doi.org/10.1177/0954405411414994
2. Verbelen, L., et al.: Characterization of polyamide powders for determination of laser sintering processability. Eur. Polym. J. **75**, 163–174 (2016). https://doi.org/10.1016/j.eurpolymj.2015.12.014
3. Goodridge, R.D., Tuck, C.J., Hague, R.J.M.: Laser sintering of polyamides and other polymers. Prog. Mater Sci. **57**(2), 229–267 (2012). https://doi.org/10.1016/j.pmatsci.2011.04.001
4. Gibson, I., Rosen, D., Stucker, B.: Direct digital manufacturing. In: Additive Manufacturing Technologies pp. 375–397. Springer, New York (2015)
5. Salmi, M.: Additive manufacturing processes in medical applications. Materials **14**(1), 191 (2021). https://doi.org/10.3390/ma14010191
6. Faustini, M.C., Neptune, R.R., Crawford, R.H., Stanhope, S.J.: Manufacture of passive dynamic ankle-foot orthoses using selective laser sintering. IEEE Trans. Biomed. Eng. **55**(2), 784–790 (2008). https://doi.org/10.1109/TBME.2007.912638
7. Telfer, S., et al.: Embracing additive manufacture: implications for foot and ankle orthosis design. BMC Musculoskelet. Disord. **13**(1), 1–9 (2012). https://doi.org/10.1186/1471-2474-13-84
8. Seppecher, P., et al.: Pantographic metamaterials: an example of mathematically driven design and of its technological challenges. Contin. Mech. Thermodyn. **31**(4), 851–884 (2019). https://doi.org/10.1007/s00161-018-0689-8
9. dell'Isola, F., et al.: Designing a light fabric metamaterial being highly macroscopically tough under directional extension: first experimental evidence. Z. Angew. Math. Phys. **66**(6), 3473–3498 (2015). https://doi.org/10.1007/s00033-015-0556-4
10. Alibert, J.J., Seppecher, P., dell'Isola, F.: Truss modular beams with deformation energy depending on higher displacement gradients. Math. Mech. Solids **8**(1), 51–73 (2003)
11. Erden Yildizdag, M., Placidi, L., Turco, E.: Modeling and numerical investigation of damage behavior in pantographic layers using a hemivariational formulation adapted for a Hencky-type discrete model. Contin. Mech. Thermodyn. 1–14 (2022)
12. Eremeyev, V.A., Turco, E.: Enriched buckling for beam-lattice metamaterials. Mech. Res. Commun. **103**, 103458 (2020)
13. Valmalle, M., Vintache, A., Smaniotto, B., Gutmann, F., Spagnuolo, M., Ciallella, A., Hild, F.: Local-global DVC analyses confirm theoretical predictions for deformation and damage onset in torsion of pantographic metamaterial. Mech. Mater. **172**, 104379 (2022)
14. Ciallella, A., Pasquali, D., D'Annibale, F., Giorgio, I.: Shear rupture mechanism and dissipation phenomena in bias-extension test of pantographic sheets: numerical modeling and experiments. Math. Mech. Solids **27**(10), 2170–2188 (2022)
15. Spagnuolo, M.: Symmetrization of mechanical response in fibrous metamaterials through micro-shear deformability. Symmetry **14**(12), 2660 (2022)
16. Golaszewski, M., Grygoruk, R., Giorgio, I., Laudato, M., Cosmo, F.D.: Metamaterials with relative displacements in their microstructure: technological challenges in 3D printing, experiments and numerical predictions. Contin. Mech. Thermodyn. **31**(4), 1015–1034 (2019)

17. Gibson, I., Shi, D.: Material properties and fabrication parameters in selective laser sintering process. Rapid Prototyp. J. **3**(4), 129–136 (1997). https://doi.org/10.1108/13552549710191836
18. Majewski, C., Zarringhalam, H., Hopkinson, N.: Effect of the degree of particle melt on mechanical properties in selective laser-sintered Nylon-12 parts. Proc. Inst. Mech. Eng. Part B J. Eng. Manuf. **222**(9), 1055–64 (2008). https://doi.org/10.1243/09544054JEM1122
19. Zarringhalam, H., Majewski, C., Hopkinson, N.: Degree of particle melt in Nylon-12 selective laser-sintered parts. Rapid Prototyp. J. **15**(2), 126–132 (2009)
20. Czelusniak, T., Amorim, F.L.: Influence of energy density on polyamide 12 processed by SLS: from physical and mechanical properties to microstructural and crystallization evolution. Rapid Prototyp. J. **27**(6), 1189–1205 (2021). https://doi.org/10.1108/RPJ-02-2020-0027
21. Starr, T.L., Gornet, T.J., Usher, J.S.: The effect of process conditions on mechanical properties of laser-sintered nylon. Rapid Prototyp. J. **17**(6), 418–423 (2011). https://doi.org/10.1108/13552541111184143
22. Amel, H., Rongong, J., Moztarzadeh, H., Hopkinson, N.: Effect of section thickness on fatigue performance of laser sintered nylon 12. Polym. Test. **53**, 204–10 (2016). https://doi.org/10.1016/j.polymertesting.2016.05.027
23. Tasch, D., Mad, A., Stadlbauer, R., Schagerl, M.: Thickness dependency of mechanical properties of laser-sintered polyamide lightweight structures. Addit. Manuf. **23**, 25–33 (2018). https://doi.org/10.1016/j.addma.2018.06.018
24. Craft, G., et al.: Impact of extended sintering times on mechanical properties in PA-12 parts produced by powderbed fusion processes. Addit. Manuf. **22**, 800–806 (2018). https://doi.org/10.1016/j.addma.2018.06.028
25. Calignano, F., Giuffrida, F., Galati, M.: Effect of the build orientation on the mechanical performance of polymeric parts produced by multi jet fusion and selective laser sintering. J. Manuf. Process. **65**, 271–82 (2021). https://doi.org/10.1016/j.jmapro.2021.03.018
26. Lammens, N., et al.: On the visco-elasto-plastic response of additively manufactured polyamide-12 (PA-12) through selective laser sintering. Polym. Test. **57**, 149–155 (2017). https://doi.org/10.1016/j.polymertesting.2016.11.032
27. Kiani, A., Khazaee, S., Badrossamay, M., Foroozmehr, E., Karevan, M.: An investigation into thermal history and its correlation with mechanical properties of PA12 parts produced by selective laser sintering process. J. Mater. Eng. Perform. **29**(2), 832–40 (2020). https://doi.org/10.1007/s11665-020-04640-0
28. Zohdi, N., Yang, R.: Material anisotropy in additively manufactured polymers and polymer composites: a review. Polymers **13**(19), 3368 (2021). https://doi.org/10.3390/polym13193368
29. Faes, M., Wang, Y., Lava, P., Moens, D.: Variability, heterogeneity, and anisotropy in the quasi-static response of laser sintered PA12 components. Strain **53**(2), e12219 (2017). https://doi.org/10.1111/str.12219
30. Mehdipour, F., Gebhardt, U., Kästner, M.: Anisotropic and rate-dependent mechanical properties of 3D printed polyamide 12-A comparison between selective laser sintering and multi jet fusion. Results Mater. **11**, 100213 (2021). https://doi.org/10.1016/j.rinma.2021.100213
31. Cobian, L., et al.: Micromechanical characterization of the material response in a PA12-SLS fabricated lattice structure and its correlation with bulk behavior. Polym. Test. **110**, 107556 (2022). https://doi.org/10.1016/j.polymertesting.2022.107556
32. Yao, B., Li, Z., Zhu, F.: Effect of powder recycling on anisotropic tensile properties of selective laser sintered PA2200 polyamide. Eur. Polym. J. **141**, 110093 (2020). https://doi.org/10.1016/j.eurpolymj.2020.110093
33. du Maire, P., Sert, E., Deckert, M., Johlitz, M., Öchsner, A.: Characterisation of the thermal ageing effects on the mechanical properties when reusing polyamide 12 in the selective laser sintering process. Materialwiss. Werkstofftech. **53**(4), 503–8 (2022). https://doi.org/10.1002/mawe.202100393
34. Zamani, M., Kadkhodaei, M., Badrossamay, M., Foroozmehr, E.: Adjustment of the scan track spacing and linear input energy to fabricate dense, pseudoelastic Nitinol shape memory alloy parts by selective laser melting. J. Intell. Mater. Syst. Struct. **33**(13), 1719–1730 (2022). https://doi.org/10.1177/1045389X211063948
35. Keshavarzan, M., Kadkhodaei, M., Badrossamay, M., Karamooz Ravari, M.R.: Investigation on the failure mechanism of triply periodic minimal surface cellular structures fabricated by Vat photopolymerization additive manufacturing under compressive loadings. Mech. Mater. **140**, 103150 (2020). https://doi.org/10.1016/j.mechmat.2019.103150
36. Rezaei, R., Karamooz Ravari, M.R., Badrossamay, M., Kadkhodaei, M.: Mechanical characterization and finite element modeling of polylactic acid BCC-Z cellular lattice structures fabricated by fused deposition modeling. Proc. Inst. Mech. Eng. C J. Mech. Eng. Sci. **231**(11), 1995–2004 (2017). https://doi.org/10.1177/0954406215626941
37. Karamooz, R.M.R., et al.: On the effects of geometry, defects, and material asymmetry on the mechanical response of shape memory alloy cellular lattice structures. Smart Mater. Struct. **25**(2), 025008 (2016). https://doi.org/10.1088/0964-1726/25/2/025008
38. dell'Isola, F., et al.: Advances in pantographic structures: design, manufacturing, models, experiments and image analyses. Contin. Mech. Thermodyn. **31**(4), 1231–1282 (2019). https://doi.org/10.1007/s00161-019-00806-x
39. Spagnuolo, M., et al.: A Green operator-based elastic modeling for two-phase pantographic-inspired bi-continuous materials. Int. J. Solids Struct. **188**, 282–308 (2020). https://doi.org/10.1016/j.ijsolstr.2019.10.018
40. Shirinbayan, M., et al.: Rotational Molding of Polyamide-12 Nanocomposites: modeling of the viscoelastic behavior. Int.J. Mater. Form. **14**(1), 143–152 (2021). https://doi.org/10.1007/s12289-020-01558-9
41. Sagradov, I., et al.: Experimental investigation and numerical modelling of 3D printed polyamide 12 with viscoplasticity and a crack model at different strain rates. Mater. Today Commun. **25**, 101542 (2020). https://doi.org/10.1016/j.mtcomm.2020.101542
42. Yang, H., Ganzosch, G., Giorgio, I., Abali, B.E.: Material characterization and computations of a polymeric metamaterial with a pantographic substructure. Z. Angew. Math. Phys. **69**(4), 1–16 (2018). https://doi.org/10.1007/s00033-018-1000-3
43. Truesdell, C., Noll, W.: The Non-linear Field Theories. Springer, Berlin (1992)
44. Pawlikowski, M.: Non-linear approach in visco-hyperelastic constitutive modelling of polyurethane nanocomposite. Mech. Time-Depend. Mater. **18**, 1–20 (2014). https://doi.org/10.1007/s11043-013-9208-2
45. Puttonen, T., Salmi, M., Partanen, J.: Mechanical properties and fracture characterization of additive manufacturing polyamide 12 after accelerated weathering. Polym. Test. **104**, 107376 (2021). https://doi.org/10.1016/j.polymertesting.2021.107376

46. Wang, H., Li, J.: Mechanical behavior evolution and damage characterization of coal under different cyclic engineering loading. Geofluids **1–19**, 2020 (2020). https://doi.org/10.1155/2020/8812188
47. Barchiesi, E., dell'Isola, F., Hild, F.: On the validation of homogenized modeling for bi-pantographic metamaterials via digital image correlation. Int. J. Solids Struct. **208**, 49–62 (2021)
48. Barchiesi, E., dell'Isola, F., Seppecher, P., Turco, E.: A beam model for duoskelion structures derived by asymptotic homogenization and its application to axial loading problems. Eur. J. Mech. A Solids **98**, 104848 (2023)
49. Giorgio, I., Hild, F., Gerami, E., dell'Isola, F., Misra, A.: Experimental verification of 2D Cosserat chirality with stretch-micro-rotation coupling in orthotropic metamaterials with granular motif. Mech. Res. Commun. **126**, 104020 (2022)